JACS
JOURNAL OF THE AMERICAN CHEMICAL SOCIETY
Communication
pubs.acs.org/JACS

Electrocatalytic Polysulfide Traps for Controlling Redox Shuttle Process of Li–S Batteries

Hesham Al Salem, Ganguli Babu, Chitturi V. Rao, and Leela Mohana Reddy Arava*

Department of Mechanical Engineering, Wayne State University, Detroit, Michigan 48202-3902, United States

Supporting Information

ABSTRACT: Stabilizing the polysulfide shuttle while ensuring high sulfur loading holds the key to realizing high theoretical energy of lithium–sulfur (Li–S) batteries. Herein, we present an electrocatalysis approach to demonstrate preferential adsorption of a soluble polysulfide species, formed during discharge process, toward the catalyst anchored sites of graphene and their efficient transformation to long-chain polysulfides in the subsequent redox process. Uniform dispersion of catalyst nanoparticles on graphene layers has shown a 40% enhancement in the specific capacity over pristine graphene and stability over 100 cycles with a Coulombic efficiency of 99.3% at a current rate of 0.2 C. Interaction between electrocatalyst and polysulfides has been evaluated by conducting X-ray photoelectron spectroscopy and electron microscopy studies at various electrochemical conditions.

The ubiquitous growth in portability of both hand-held electronics as well as electric vehicles has largely been fueled by the progress made in electrochemical energy storage. Li-ion batteries have been at the forefront of this energy storage transformation, however, if the future energy needs are taken into account, the current pace of technological progress will be unable to sustain the demand.[1,2] Beyond the limitations of Li-ion batteries, the lithium–sulfur (Li–S) system is a promising electrochemical energy storage technology due to its low cost, high theoretical energy density, safety, and eco-friendliness.[1] However, practical applications of the Li–S battery are hindered by a multitude of issues like short cycle life, poor Coulombic efficiency, poisoning of Li-anode, self-discharge, etc.[3] The underlying primary reason behind these performance barriers is the well-known polysulfide shuttle mechanism, a process initiated in the preliminary stages of battery discharging. This mechanism results in dissolution of polysulfides (PS) into the electrolyte solution causing undesirable mass transport of electroactive species resulting in the formation of a passivation layer on the Li-anode.[4] Insulating nature of sulfur and its end products of discharge (Li_2S_2 and Li_2S) further leads to slow charge/discharge process and increases in cell polarization.[5,6] Barchasz et al.[7] and others[8−11] reported that passivation of the cathode surface by insoluble byproducts and poor adsorption of soluble PS are the primary reason for poor performance of Li–S batteries.[12]

To tackle the above-mentioned challenges, a majority of recent research efforts have been directed toward designing polymer electrolytes that prevent the migration of PS[13,14] and surface coatings on Li-anode to avoid PS passivation,[15,16] and on the other hand, carbon materials for improving conductivity of sulfur and trapping intermediate PS with the cathode of the cell.[17,18] In search of finding carbon hosts for PS, several micro/mesoporous structures, carbon nanotubes, graphene, etc.[19−21] have been investigated thoroughly. The poor adsorption capabilities of carbons toward polar natured PS[22] have further triggered research interest in finding alternative host materials.[12,22−25] Moreover, the PS conversion reaction kinetics worsens with prolonged cycling due to an increase in internal resistance caused by deposition of insulating short-chain PS. In marked contrast to all the above-mentioned approaches, we have recently demonstrated that the PS shuttle process in Li–S cell can be controlled by means of electrocatalysis.[26] Use of electrocatalytic current collectors such as Pt or Ni when coated on Al foil has shown to enhance both cycle life and reaction kinetics of the Li–S battery.[26] Despite the fact that surface chemistry of metal thin films enhances the PS anchoring strength, active material loading is limited due to constrained surface area. In order to effectively utilize catalysts (Pt and Ni) while ensuring high surface area to host PS, the present study is aimed at understanding the structural and electrochemical properties of graphene supported nanocatalysts. The high surface area, superior mechanical and electrical properties, electrochemical compatibility and its prior attempts to host sulfur cathode make graphene an ultimate choice for supporting electrocatalysts.[27]

The step-by-step process of graphene nanocomposites preparation and their interaction with lithium PS (LiPS) during charge/discharge process is illustrated schematically in Figure 1.

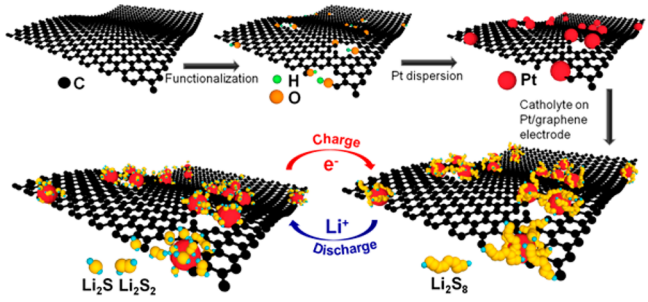

Figure 1. Schematic illustration of electrocatalyst anchored graphene nanocomposite preparation and its interaction with PS during charge/discharge process of the Li–S battery.

Received: April 29, 2015
Published: September 2, 2015

DOI: 10.1021/jacs.5b04472
J. Am. Chem. Soc. 2015, 137, 11542−11545

For the synthesis of such composites, first, chemical functionalization of few layer graphene was performed in a reflux condenser using concentrated nitric acid at 120 °C under the Ar flow. Pt and Ni nanoparticles are dispersed uniformly on such functionalized graphene sheets to increase their surface anchoring strength (see Supporting Information).[28] Field emission scanning electron spectroscopy (FESEM) images and elemental mapping of Ni/graphene and Pt/graphene are shown in Figure 2a–d. Randomly oriented graphene sheets of few-

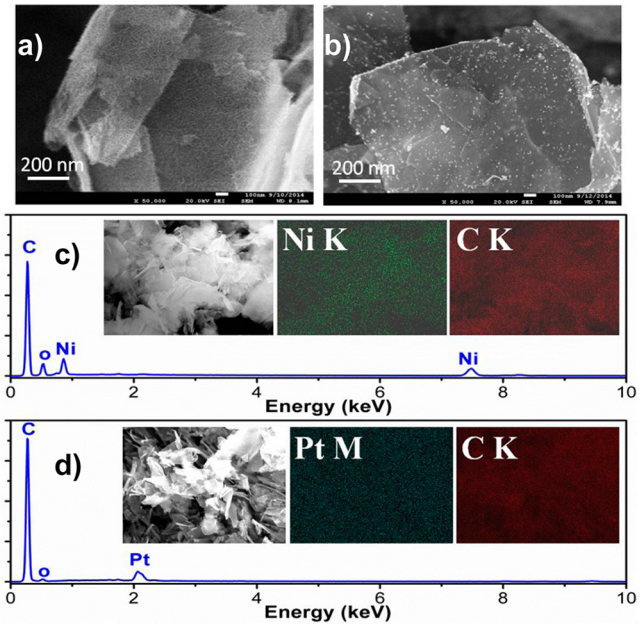

Figure 2. Characterization of nanocomposites: (a and b) FESEM images and (c and d) EDX and elemental mapping (inset) of Ni and Pt nanoparticles anchored graphene layers prepared by polyol process, respectively.

microns in size and ripple-like flake morphology (Figure S1) are depicted in FESEM images. In the case of Ni/graphene and Pt/graphene composites, a spatial distribution of metallic nanoparticles about 20 nm in size over the layered graphene sheets was observed (Figure 2a,b). Further, energy dispersive X-ray spectroscopic (EDX) analysis confirmed the homogeneous distribution of respective elements (Figure 2c,d). From X-ray diffraction studies (XRD), it is determined that the interspacing distance between graphene layers is 3.34 Å and crystal structure of electrocatalyst is face-centered cubic (Figure S2).

To evaluate the electrochemical performance of graphene and its nanocomposites, standard 2032 coin cells were fabricated using them as a cathode vs metallic lithium as an anode and dissolved Li_2S_8 in electrolyte (catholyte) as an active material. For better comparison, parameters such as concentration and quantity of catholyte (0.6 M and 10 μL) during cell fabrication have been maintained constant. Galvanostatic charge/discharge studies were performed at a constant current rate of 0.1 C (based on sulfur mass in the cell), and obtained results for 100 cycles are displayed in Figure 3. From Figure 3a, it was observed that electrodes exhibited well-defined discharge plateaus corresponding to the formation of soluble long-chain PS and their spontaneous dissociation into short-chain PS and vice versa during the charging process. On careful observation, Pt/graphene electrode shows two discharge plateaus at 2.4 and 1.97 V and a charging plateau at 2.34 V. Ni/graphene and Pt/

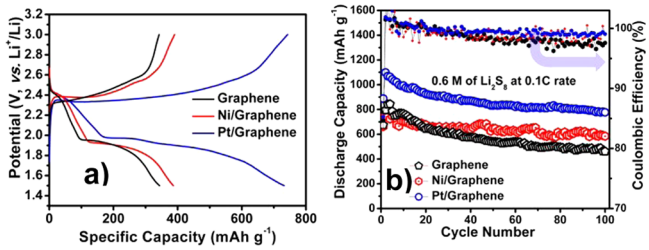

Figure 3. Electrochemical performance: (a) voltage vs specific capacity profile and (b) galvanostatic charge/discharge behavior and Coulombic efficiency of pristine and electrocatalyst anchored graphene electrodes vs Li^+/Li at 0.1C rate in the potential range of 1.5–3.0 V.

graphene electrodes exhibit an initial specific capacity of 740 and 1100 mAh g^{-1} and retain a stable capacity of 580 and 789 mAh g^{-1} after 100 cycles of charge/discharge. In comparison with pristine graphene, Ni/graphene and Pt/graphene resulted in 20% and 40% enhancement in capacity, respectively. More notably, Pt/graphene electrode showcases excellent stability in Coulombic efficiency (~99.3%) upon cycling (Figure 3b). Thus, Pt is promising as an electrocatalyst to convert short- to long-chain LiPS efficiently in a kinetically facile manner during charging. The deposition of insulating PS on graphene impedes the electron transfer at the electrode/electrolyte interface and results in an increase of internal resistance. In case of electrocatalyst anchored graphene, the presence of catalyst (Pt or Ni) helps to convert these PS deposits back to soluble long-chain PS and hence enhances reaction kinetics and retains high Coulombic efficiency. As Pt/graphene is found to exhibit superior performance over Ni/graphene and graphene (Table S1), further studies have been focused on evaluating its electrocatalytic properties and its possible interactions with LiPS during the cycling process.

In order to validate the electrocatalytic activity of Pt/graphene over pristine graphene, cyclic voltammograms (CVs) were recorded at a slow scan rate of 0.05 mV s^{-1} (Figure 4a). Similar to

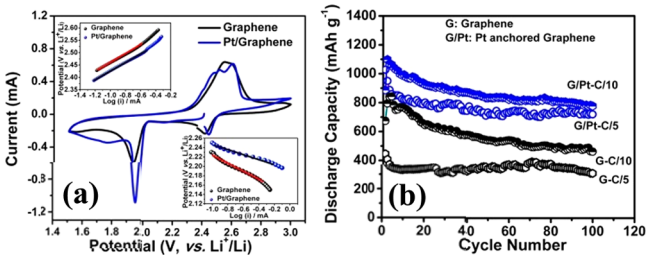

Figure 4. Evaluation of catalytic properties: (a) CVs of graphene and Pt/graphene electrodes at a scan rate of 0.05 mV s^{-1} (inset: Tafel plots for corresponding oxidation and reduction reactions) and (b) cyclic stability and C-rate tests of Pt/graphene electrodes.

charge/discharge profiles, two characteristic reduction peaks (cathodic) observed on CV correspond to the disproportion of long-chain PS and formation of Li_2S_2 and Li_2S respectively. On forward scan, broad oxidation peak at 2.57 V for pristine graphene is attributed to the conversion of short-chain to long-chain LiPS. However, the CV of Pt/graphene displays two distinguishable oxidation peaks that evidence the better reversibility of reaction at a given scan rate. When the CV of Pt/graphene is compared to that of graphene, the distinguishable positive shift in reduction peak and negative shift in oxidation peak indicate the superior catalytic activity of Pt-containing

DOI: 10.1021/jacs.5b04472
J. Am. Chem. Soc. 2015, 137, 11542–11545

electrode toward the LiPS conversion process (Table S2). These peak shifts typically indicate a decrease in cell polarization, which is in good agreement with galvanostatic charge/discharge profiles shown in Figure 3a. Further, Tafel plots and corresponding exchange current density values have been derived from potentiostatic polarization experiments to understand the effect of catalyst on charge-transfer kinetics during the charge and discharge reaction process (inset of Figure 4a). The calculated exchange current densities (i_0) of pristine and Pt/graphene electrodes are 1.18 and 3.18 mA cm^{-2} for the cathodic process and 0.17 and 0.29 mA cm^{-2} for the anodic process, respectively (Table S2). Thus, the increase in exchange current density values of Pt/graphene in both charge and discharge processes confirms the enhancement in rate of LiPS conversion reactions. Further, electrochemical impedance spectra (EIS) were recorded to envisage the electrocatalyst influence on charge-transfer resistance. Figure S3 shows the typical Nyquist plots measured before and after 10 charge/discharge cycles. An inferior electrode/electrolyte interface resistance for Pt/graphene (60 Ω) over pristine graphene electrode (170 Ω) has been observed. Furthermore, EIS of pristine graphene exhibits an extra-flattened semicircle, which could be due to the deposition of insoluble products on electrode surface. Hence, reduced redox peak separation, higher exchange current density, and minimal electrode/electrolyte resistance are clearly in agreement with the claimed catalysis of PS in the presence of Pt/graphene electrode.

Electrochemical behavior of graphene and Pt/graphene electrodes at different C-rates was performed to reveal the surface anchoring strength of electrocatalyst toward PS conversions. As shown in Figure 4b, Pt/graphene electrode delivers superior specific capacity compared to that of pristine graphene electrode at both C/5 and C/10. For instance, the discharge capacity of 780 mAh g^{-1} was exhibited by Pt/graphene electrode at 0.2 C for 100 cycles. This is almost double that of graphene (380 mAh g^{-1}) under similar conditions. The Pt/graphene electrode was further subjected to long cycling (about 300 cycles) at 1C-rate and exhibited a stable performance with minimal capacity loss of 0.09% per cycle (Figure S4). Voltage vs capacity plot for the Pt/graphene electrode shows typical discharge and charge plateaus at high current rates (Figure S5). The charging plateau relies more on the electrochemical activity of cathode material which includes conversion of short-chain to long-chain LiPS. The consistency in charging plateaus, even with high C-rates, suggests the enhanced reaction kinetics due to presence of electrocatalyst. To understand the feasibility of Pt/graphene electrode toward high sulfur loading, higher molar concentrations of catholyte containing 0.8 and 1.0 M Li_2S_8 (corresponds to 1.61 and 2.0 mg of sulfur per cm^{-2}, respectively) were prepared and subjected to electrochemical studies. Herein, Pt/graphene electrode exhibits specific capacities of 550 and 410 mAh g^{-1} with 0.8 and 1.0 M of Li_2S_8, respectively, at 0.2 C-rate with stability over 100 cycles (Figure S6). In order to validate electrocatalyst sensitivity toward temperature, the cell containing the Pt/graphene electrode was first cycled at room temperature (RT) for 5 cycles and then cycled at 60 °C. In agreement with electrocatalysis behavior, Pt/graphene electrode showed significantly reduced polarization at 60 °C compared to RT with enhanced specific capacity (Figure S7).

The interaction between electrocatalyst and PS during the charge and discharge process was probed by conducting FESEM, XRD, and X-ray photoelectron spectroscopy (XPS) studies on cycled cells. Electrodes are decrimped carefully from 2032 coin cells, washed thoroughly with tetraethylene glycol dimethyl ether solvent, and dried in vacuum for 12 h. After five charge/discharge cycles, both graphene and Pt/graphene electrodes are examined in discharge and charge states separately. FESEM images of graphene and Pt/graphene electrodes at the charged state are shown in Figure 5a,b, respectively. The presence of precipitated

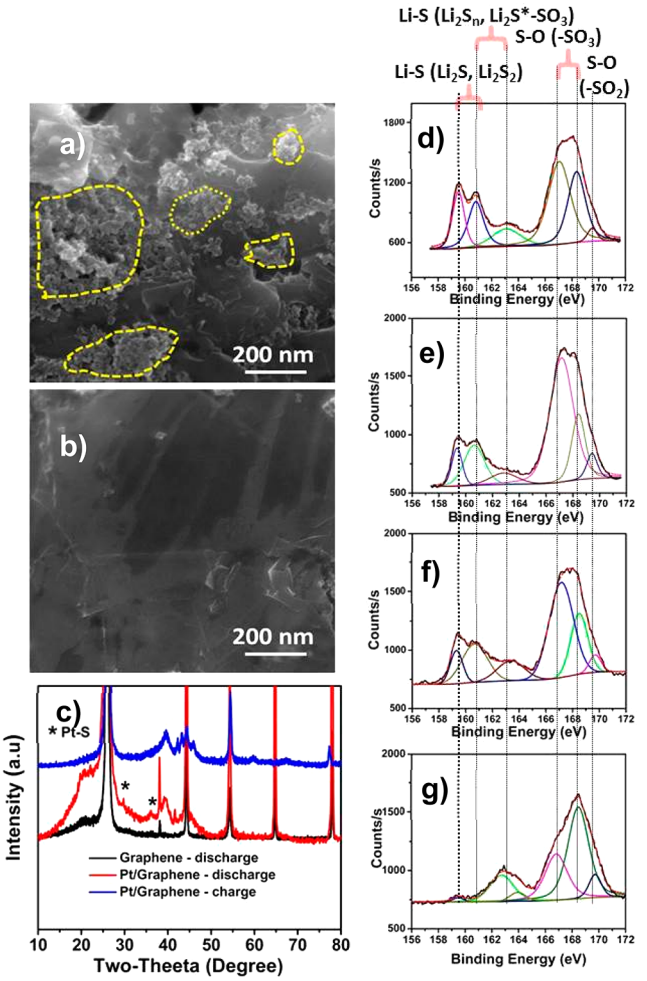

Figure 5. Pt−PS interactions: FESEM images reveal the large amount of insoluble LiPS deposition on (a) pristine graphene (highlighted in yellow circles) and (b) reduced amount of LiPS species on Pt anchored graphene, (c) enlarged XRD patterns of pristine and Pt anchored graphene electrode, and XPS analysis (S_{2p}) of pristine graphene (d and e) and Pt/graphene electrodes (f and g) in discharged and charged state, respectively.

insoluble LiPS (some of them are marked with broken yellow lines) in graphene electrode and its significant reduction in Pt/graphene is further evidence that catalyst helps to keep the electrode structure active even after several cycles of the charge/discharge process (Figure S8). From XRD patterns, formation of platinum sulfide on the discharged state (2θ = 29.2° and 36.4°) and further its fading on charging (Figures 5c and S9) was observed. Hence, it is confirmed that the nature of interactions between Pt and sulfur is reversible and accountable for stable electrochemical performance.[29,30]

Further, XPS spectra for graphene and Pt/graphene electrodes at discharged and charged states were recorded to understand Pt−PS interactions. From Figure 5d−g, XPS spectra of deconvoluted S_{2p} peaks at 159.3 eV, corresponding to the

DOI: 10.1021/jacs.5b04472
J. Am. Chem. Soc. 2015, 137, 11542−11545

formation of insoluble Li_2S and Li_2S_2 products observed in both discharge and charged states of graphene electrode. The presence of such peaks in the charged state indicates poor reversibility of deposited short-chain to long-chain PS. On the other hand, significant reduction in the relative area of the XPS peak observed for the charged state of Pt/graphene electrode witnesses the better reversibility (Table S3).[12,24,31] The positive shift in other two peaks of Pt (charged state) at 162.7 and 163.9 eV is ascribed to S−O and S−S bands, especially later evidence of the formation of elemental sulfur with respect to Pt/graphene. Furthermore, from the deconvoluted 4f7/2 and 4f5/2 peaks of Pt (Figure S10), the presence of Pt^{2+} species indicates interactions with LiPS products during discharge.[32] Decrease in the presence of Pt^{2+} compared to its counterpart Pt^0 during the charge process further supports the argument that Pt aids bonding of LiPS species on electrode surface during the discharge process and helps the reversible reaction during charging process. Hence, Pt nanoparticle plays a crucial role in adsorbing PS species during the discharge process and further converts them into long-chain LiPS and elemental sulfur during the charging process. As a proof of concept, similar experiments, as a feasibility of extending this concept to a non-noble metal catalysts, have been conducted by taking bulk WC and TiC as electrodes against PS-based electrolyte (Figure S11).

In summary, we bring electrocatalysis principles to the Li−S battery configuration to stabilize the PS shuttle process and to enhance the rate capabilities. Pt/graphene and Ni/graphene have exhibited reduced overpotential and excellent specific capacity over pristine graphene electrodes. More importantly, presence of electrocatalyst (Pt) helps to demonstrate a 40% enhancement in the specific capacity over pristine graphene with a Coulombic efficiency above 99.3%. Postmortem analysis of electrodes further confirms the catalyst affinity toward adsorbing soluble PS and converting them into long-chain PS without allowing them to precipitate much on the electrode. Thus, introducing a catalyst in the Li−S system will open a new avenue for improving electrochemical performance.

■ ASSOCIATED CONTENT

Supporting Information

The Supporting Information is available free of charge on the ACS Publications website at DOI: 10.1021/jacs.5b04472.

Experimental details and additional data (PDF)

■ AUTHOR INFORMATION

Corresponding Author

*leela.arava@wayne.edu

Notes

The authors declare no competing financial interest.

■ ACKNOWLEDGMENTS

L.M.R.A. acknowledges the support from Wayne State University faculty startup funds.

■ REFERENCES

(1) Bruce, P. G.; Freunberger, S. A.; Hardwick, L. J.; Tarascon, J. M. *Nat. Mater.* **2012**, *11*, 19.

(2) Manthiram, A.; Fu, Y.; Chung, S.-H.; Zu, C.; Su, Y.-S. *Chem. Rev.* **2014**, *114*, 11751.

(3) Mikhaylik, Y. V.; Akridge, J. R. *J. Electrochem. Soc.* **2004**, *151*, A1969.

(4) Zhang, S. S. *J. Power Sources* **2013**, *231*, 153.

(5) Schneider, H.; Garsuch, A.; Panchenko, A.; Gronwald, O.; Janssen, N.; Novák, P. *J. Power Sources* **2012**, *205*, 420.

(6) Jayaprakash, N.; Shen, J.; Moganty, S. S.; Corona, A.; Archer, L. A. *Angew. Chem.* **2011**, *123*, 6026.

(7) Barchasz, C.; Leprêtre, J.-C.; Alloin, F.; Patoux, S. *J. Power Sources* **2012**, *199*, 322.

(8) Cheon, S.-E.; Ko, K.-S.; Cho, J.-H.; Kim, S.-W.; Chin, E.-Y.; Kim, H.-T. *J. Electrochem. Soc.* **2003**, *150*, A800.

(9) Li, L.; Ruan, G.; Peng, Z.; Yang, Y.; Fei, H.; Raji, A.-R. O.; Samuel, E. L. G.; Tour, J. M. *ACS Appl. Mater. Interfaces* **2014**, *6*, 15033.

(10) Xu, R.; Belharouak, I.; Zhang, X.; Chamoun, R.; Yu, C.; Ren, Y.; Nie, A.; Shahbazian-Yassar, R.; Lu, J.; Li, J. C. M.; Amine, K. *ACS Appl. Mater. Interfaces* **2014**, *6*, 21938.

(11) Li, W.; Hicks-Garner, J.; Wang, J.; Liu, J.; Gross, A. F.; Sherman, E.; Graetz, J.; Vajo, J. J.; Liu, P. *Chem. Mater.* **2014**, *26*, 3403.

(12) Demir-Cakan, R.; Morcrette, M.; Nouar, F.; Davoisne, C.; Devic, T.; Gonbeau, D.; Dominko, R.; Serre, C.; Férey, G.; Tarascon, J.-M. *J. Am. Chem. Soc.* **2011**, *133*, 16154.

(13) Wu, F.; Chen, J.; Chen, R.; Wu, S.; Li, L.; Chen, S.; Zhao, T. *J. Phys. Chem. C* **2011**, *115*, 6057.

(14) Li, G.-C.; Li, G.-R.; Ye, S.-H.; Gao, X.-P. *Adv. Energy Mater.* **2012**, *2*, 1238.

(15) Ma, G.; Wen, Z.; Wu, M.; Shen, C.; Wang, Q.; Jin, J.; Wu, X. *Chem. Commun.* **2014**, *50*, 14209.

(16) Ma, G.; Wen, Z.; Wang, Q.; Shen, C.; Jin, J.; Wu, X. *J. Mater. Chem. A* **2014**, *2*, 19355.

(17) Yang, X.; Zhang, L.; Zhang, F.; Huang, Y.; Chen, Y. *ACS Nano* **2014**, *8*, 5208.

(18) Xu, J.; Shui, J.; Wang, J.; Wang, M.; Liu, H.-K.; Dou, S. X.; Jeon, I.-Y.; Seo, J.-M.; Baek, J.-B.; Dai, L. *ACS Nano* **2014**, *8*, 10920.

(19) Fang, R.; Zhou, G.; Pei, S.; Li, F.; Cheng, H.-M. *Chem. Commun.* **2015**, *51*, 3667.

(20) Bonaccorso, F.; Colombo, L.; Yu, G.; Stoller, M.; Tozzini, V.; Ferrari, A. C.; Ruoff, R. S.; Pellegrini, V. *Science* **2015**, *347*, 6217.

(21) Li, Z.; Jiang, Y.; Yuan, L.; Yi, Z.; Wu, C.; Liu, Y.; Strasser, P.; Huang, Y. *ACS Nano* **2014**, *8*, 9295.

(22) Pang, Q.; Kundu, D.; Cuisinier, M.; Nazar, L. F. *Nat. Commun.* **2014**, *5*, 4759.

(23) Liang, X.; Hart, C.; Pang, Q.; Garsuch, A.; Weiss, T.; Nazar, L. F. *Nat. Commun.* **2015**, *6*, 5682.

(24) Yang, Y.; Yu, G.; Cha, J. J.; Wu, H.; Vosgueritchian, M.; Yao, Y.; Bao, Z.; Cui, Y. *ACS Nano* **2011**, *5*, 9187.

(25) Tao, X.; Chen, F.; Xia, Y.; Huang, H.; Gan, Y.; Chen, X.; Zhang, W. *Chem. Commun.* **2013**, *49*, 4513.

(26) Babu, G.; Ababtain, K.; Ng, K. Y. S.; Arava, L. M. R. *Sci. Rep.* **2015**, *5*, 8763.

(27) Yan, Z.; He, G.; Jiang, Z.; Wei, W.; Gao, L.; Xie, J. *J. Power Sources* **2015**, *284*, 497.

(28) Xu, C.; Wang, X.; Zhu, J. *J. Phys. Chem. C* **2008**, *112*, 19841.

(29) Chi Linh, D.; Thy San, P.; Ngoc Phong, N.; Viet Quan, T. *Adv. Nat. Sci.: Nanosci. Nanotechnol.* **2013**, *4*, 035011.

(30) Song, J.; Gordin, M. L.; Xu, T.; Chen, S.; Yu, Z.; Sohn, H.; Lu, J.; Ren, Y.; Duan, Y.; Wang, D. *Angew. Chem., Int. Ed.* **2015**, *54*, 4325.

(31) Diao, Y.; Xie, K.; Xiong, S.; Hong, X. *J. Electrochem. Soc.* **2012**, *159*, A1816.

(32) Yung, T.-Y.; Lee, J.-Y.; Liu, L.-K. *Sci. Technol. Adv. Mater.* **2013**, *14*, 035001.

DOI: 10.1021/jacs.5b04472
J. Am. Chem. Soc. 2015, 137, 11542−11545